4f/5d hybridization in the heavy rare earth elements Er and Tm

S. D. Brown,[1,3] P. Strange,[2] L. Bouchenoire,[1,3] and P. B. J. Thompson[1,3]

[1]*XMaS, European Synchrotron Radiation Facility, 6 rue Jules Horowitz, BP220, 38043 Grenoble, France*
[2]*School of Physical Sciences, University of Kent, Canterbury, Kent, CT2 7NH, United Kingdom*
[3]*Department of Physics, University of Liverpool, Oliver Lodge Laboratory, Oxford Street, Liverpool, L69 7ZE, United Kingdom*

We present experimental data and first-principles calculations of the x-ray resonant magnetic scattering (XRMS) line shapes of Er and Tm metals. Band structure calculations are presented that illustrate the existence of 4f/5d hybridization of unoccupied electron levels. This leads to spin and orbital features in the XRMS spectra that are not representative of the 5d occupied moments. General trends through the heavy rare earth series are discussed with reference to previous work.

More than two decades have passed since x-ray resonant magnetic scattering (XRMS) experiments were first performed on the heavy rare earths. Following the prediction of the possibility of large resonant enhancements of magnetic scattering at the L absorption edges,[1] the effect was first observed in the antiferromagnetic phases of Ho.[2,3] These spectra were interpreted in terms of an atomic model, with electric dipole transitions ($E1$) from the 2p core levels to the unoccupied 5d levels and electric quadrupole transition ($E2$) from the same core levels to the unoccupied 4f levels.[4] This model was later rewritten explicitly in terms of the angular dependences[5] with the approximation of spherical symmetry and more recently to include the noncentrosymmetric case applicable to all of the hexagonal close-packed heavy rare earths.[6] In early x-ray spectroscopic studies,[2,3,7–12] the lower-energy peaks were generally interpreted as $E2$ and the higher energy ones as $E1$, due to the predicted polarization and angular dependences of the observed features.

However, recent density functional theory (DFT) calculations and experimental results using charge-magnetic x-ray resonant interference scattering (XRIS) in the ferri- and ferromagnetic phases of the heavy rare earth metals have challenged the standard interpretation, predicting and experimentally demonstrating the presence of $E1$ transitions both at the higher energy and at the lower energy in addition to the $E2$ transitions.[13,14] The presence of the low-energy $E1$ contribution was attributed to hybridization between the unoccupied f and d states just above the Fermi energy. The band structure calculations showed antiparallel unoccupied f-d spin hybridization, providing an alternative interpretation of the dispersive line shape observed in x-ray magnetic circular dichroism (XMCD) spectra from the heavy rare earths.

To date, XRMS measurements on third-generation synchrotrons have demonstrated the existence of such low-energy $E1$ transitions in the antiferromagnetic phases of Tb[15] and Ho,[16] through angular and polarization dependence studies combined with band structure calculations. Here, we present experimental and theoretical confirmation of the presence of the lower-energy $E1$ feature in the antiferromagnetic XRMS spectra of Er and Tm. First-principles fully relativistic electronic structure and scattering calculations are used to elucidate the origin of the low-energy $E1$ mixed f-d features. A simple

model of the scattering based on the calculated spin and orbital polarizations and their Kramers-Kronig transforms is also employed in order to highlight the effect of matrix elements on the calculated spectra. Early XRMS measurements of Tm[17] and Er[18] were carried out on X22C at the National Synchrotron Light Source (NSLS), where the energy resolution was around a factor of four lower than for the results reported here. As a consequence, the fine structures of the resonances could not be resolved. In the case of Tm, these results have implications for the interpretation of previous XRMS data from the mixed valence compound TmSe,[19] highlighting the importance of inclusion of the low-energy $E1$ contribution in the analysis of XRMS from rare earth systems.

The experiments reported here were performed at the XMaS beamline[20] BM28 at the European Synchrotron Radiation Facility (ESRF). The Si(111) double-bounce monochromator was tuned to the L_{III} edge of each rare earth, providing horizontally polarized radiation in a bandwidth of around 1.5 eV. The (001) surface cut Er and Tm single crystals were grown by D. Fort at the University of Birmingham, United Kingdom, allowing diffraction to be performed from the c axis faces. They were the same samples employed in our earlier XRIS study.[13] The samples were mounted in a closed cycle refrigerator with a base temperature of around 10 K. Both Tm and Er have c axis modulated (CAM) antiferromagnetic structures at appropriate temperatures ($T < 25$ K for Tm and 52 K $< T <$ 85 K for Er), and the results reported in the following were obtained within these CAM phases. The (006-τ) magnetic satellites (where τ is the antiferromagnetic modulation wave vector) were monitored while scattering horizontally through angles close to 90° (2$\theta = 98.4°$ for Er and 95.1° for Tm). Polarization analysis was performed in order to isolate the $\pi \rightarrow \pi$ and $\pi \rightarrow \sigma$ magnetic scattering channels with a Cu(222) analyzer crystal employed for Er and a LiF(400) analyzer crystal for Tm. Energy scans were performed by varying the incident energy and adjusting the diffractometer angles accordingly in order to maintain the diffraction condition.

Spectra were calculated using a fully relativistic theory of XRMS based on DFT and implemented using the Linear Muffin-Tin Orbital method in the Atomic Sphere Approximation (LMTO-ASA)[21] band structure method. This enables us to include all matrix elements in the calculation
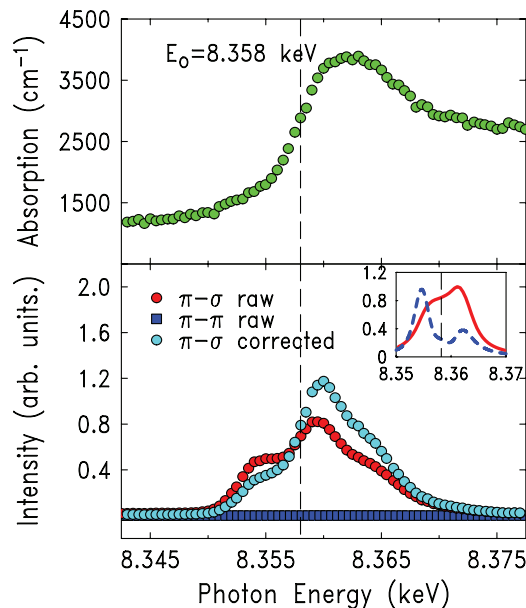
FIG. 1. (Color online) Er absorption measured through a 5-μm-thick foil and rescaled to tabulated values (upper panel). The inflection point is labeled as E_0. In the lower panel, we show the raw data for the (006-τ) magnetic reflection for both $\pi \rightarrow \sigma$ and $\pi \rightarrow \pi$ channels as well as the $\pi \rightarrow \sigma$ absorption-corrected data. The inset of the lower panel shows the relativistic DFT results (red, solid) and also the simple model results that do not include the energy dependence of the matrix elements (blue, dashed).

FIG. 2. (Color online) Tm absorption measured through a 5-μm-thick foil and rescaled to tabulated values (upper panel). The inflection point is labeled as E_0. In the lower panel, we show the raw data for the (006-τ) magnetic reflection for both $\pi \rightarrow \sigma$ and $\pi \rightarrow \pi$ channels as well as the $\pi \rightarrow \sigma$ absorption-corrected data. The inset of the lower panel shows the results of the relativistic DFT (red, solid) and also the simple model results that do not include the energy dependence of the matrix elements (blue, dashed).

straightforwardly.[22,23] The calculation used the local-density approximation for exchange correlation and 1536 k points in the Brillouin zone. Further details of the method are reported elsewhere.[24,25]

The XRMS spectra for Er and Tm are shown in Figs. 1 and 2. The upper panels show the absorption measured on transmission through 5-μm foils and rescaled to tabulated values. The energy dependence of the (006-τ) antiferromagnetic reflections were measured in both the $\pi \rightarrow \sigma$ and $\pi \rightarrow \pi$ channels, with $\tau = 0.289(5)$ c* for Er at 53 K and 0.285(7) c* for Tm at 14 K, and are shown in the lower panels of Figs. 1 and 2, along with absorption corrected data. For CAM magnetic structures, where the moments are sinusoidal along the c axis, only the $E1$ and $E2$ $\pi \rightarrow \sigma$ channels are allowed at the first magnetic satellite, where the individual contribution are given by[5,6]

$$f_{E_1, 1st}^{XRMS}(\pi - \sigma) = -F_{E_1}^{(1)} \frac{1}{2} \sin \theta \qquad (1)$$

$$f_{E_2, 1st}^{XRMS}(\pi - \sigma) = -\frac{3}{8} \sin \theta \left[\left(F_{E_2}^{(3)} + \frac{5}{6} F_{E_2}^{(1)} \right) \cos 2\theta + \frac{1}{2} F_{E_2}^{(1)} \right] \qquad (2)$$

where $F_{E_1}^{(1)}$ and $F_{E_2}^{(n)}$ are a combination of Clebsch-Gordan coefficients, the resonant energy denominator, and the radial dipole or quadrupole matrix elements, respectively, and are independent of scattering geometry.[5,6] In Eq. (2), the $E2$ terms multiplied by $\cos 2\theta$ will be negligible for the scattering angles involved here, and the final first-order term will dominate, which is reduced by a factor of 3/8 compared to the $E1$ amplitude in Eq. (1). Thus, the $E2$ intensity will be at least a factor of 7 less than that of the $E1$ [assuming, in the worst
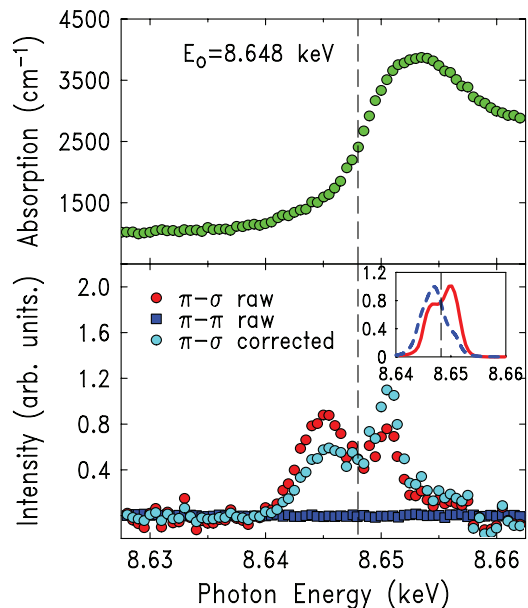
case, similar values for $F_{E_1}^{(1)}$ and $F_{E_2}^{(1)}$]. It is clear then that the lower-energy peaks in Figs. 1 and 2 cannot be attributed to $E2$ scattering. Also, $E1$-$E2$ scattering can be ruled out as this can only occur at satellites around odd values of l.[6] We therefore conclude that the experimentally observed $\pi \rightarrow \sigma$ scattering is predominantly of $E1$ origin. The insets of Figs. 1 and 2 show the results of our DFT calculations in red and in blue, a simple model described in Ref. 13 based on theoretical spin and orbital polarizations and their Kramers-Kronig transforms, which does not take into account the energy dependence of the matrix elements. Although properly including the energy dependence of the matrix elements, as in our DFT calculations, gives closer agreement with experiment, it is true that the double-peak structure is obtained even with the simple model, thus establishing a link between the DFT results and the more familiar spin and orbital polarization. The XRMS study of TmSe[19] was performed on X16B at NSLS, where the energy resolution was similar to that of the present study and a split magnetic resonance at the Tm L_{III} edge was observed. The presence of the double-peak structure was taken as unambiguous establishment that long-range magnetic order was present for both the Tm^{2+} and Tm^{3+} valence states in this mixed-valence compound. However, our current results show that Tm metal also exhibits an extremely similar double-peaked structure, and therefore the existence of long-range magnetic order in both valence states of TmSe remains an open question.

In Fig. 3, we show the $5d$ unoccupied densities of states (DOSs) for Tm (the DOS for Er being very similar), decomposed by spin and orbital moments, together with the
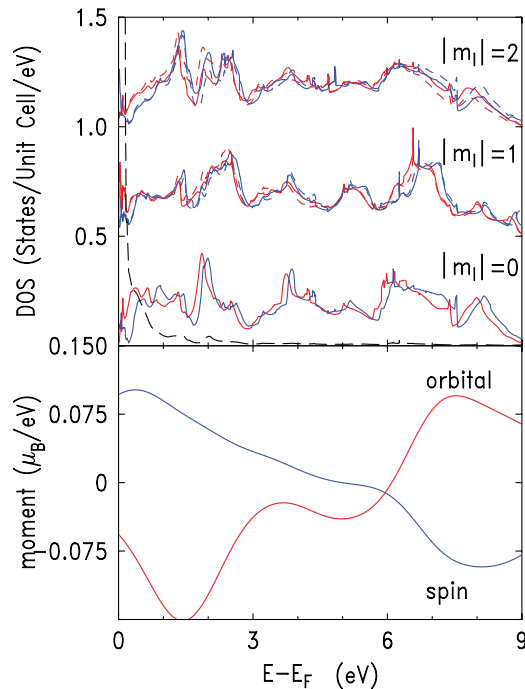
FIG. 3. (Color online) Tm 5*d* unoccupied DOS plotted for $|m_l|$ (each offset by 0.5). The spin-up states are in red and the spin down in blue. Positive m_l are solid and negative m_l dashed (upper panel). The black dashed line shows the unoccupied 4*f* DOS. In the lower panel, we show the 3-eV convoluted spin and orbital 5*d* unoccupied moments.
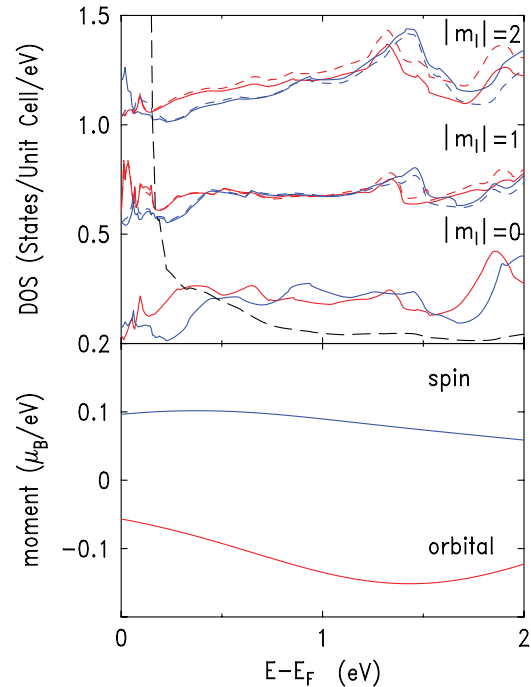

FIG. 4. (Color online) Expanded view of the low-energy region of the Tm DOS in Fig. 3, plotted for $|m_l|$ (each offset by 0.5). The spin-up states are in red and the spin down in blue. Positive m_l are solid and negative m_l dashed (upper panel). The black dashed line shows the unoccupied 4*f* DOS. In the lower panel, we show the 3-eV convoluted spin and orbital moments.

unoccupied 4*f* DOS. The lower panel shows the total 5*d* unoccupied spin and orbital moments, convoluted with a 3-eV Lorentzian, as a function of energy. As expected, the 5*d* DOSs display three distinct forms, depending on $|m_l|(=0; 1$ or 2). These data tell us which states are responsible for both the spin and orbital contribution to the total moments. For example, the difference between the two curves $|m_l| = 2$ for spin up shows the contribution of these states to the orbital moment. For $m_l = 0$, there is no orbital moment, and above 1 eV, there is an approximate rigid shift upwards of the minority spin states that represents the spin contribution from these states to the total moment. Figure 4 shows an expanded view of the low-energy region of Fig. 3. Below 1 eV, the behavior becomes rapidly varying due to the mixing of the 5*d* states with the unoccupied 4*f* states lying just above the Fermi energy (E_F). This mixing is key to determining the indirect exchange interaction between the ions and hence the magnetic ordering. The peaks in the spin moments just above E_F are due to hybridization of the empty majority spin *d* states and minority spin *f* states. This yields a positive spin moment at relatively low energies, which then has to be compensated by a negative spin moment at higher energies. At energies just above E_F, the coupling of the 4*f* and the 5*d* orbital moments are parallel and again this has to be compensated at higher energies. The detailed structure in these curves can be attributed to the crystal field and to the influence of the 6*s* states. In a previous publication,[13] we have shown how these curves influence the magnetic scattering of x rays. Looking more closely at the region from ~0.25 to ~0.75 eV above E_F, we see that for all values of m_l the spin-up 5*d* DOS is greater than that for spin down. The negative peak in the orbital

moment at around 1.4 eV is dominated by $|m_l| = 2$, although there is also a significant contribution from the $|m_l| = 1$ states. It has been noted before in Ref. 26 that most of the structure in the x-ray scattering from rare earth L_{III} edges can be attributed to $|m_l| = 2$ states, and our results support this conclusion. The hybridized positive peak in the 5*d* spin-polarized DOS and its negative closure peak at higher energies thus contribute significantly to the dispersive line shapes observed in XMCD measurements, in addition to the dispersive contribution from the exchange splitting. In the region of 5*d*/4*f* overlap (0 to ~0.25 eV), the states are very mixed, and no particular orbital coupling dominates in this energy range. However, our results show that $m_l = +2$ is dominated by spin down, and $m_l = +1$ is mainly spin up in this region. Above 1 eV, spin splitting of the states becomes discernible.

In general, the L_2/L_3 branching ratio is not calculated correctly unless spin-orbit coupling is included in the 5*d* band. The work of Lee and coworkers[26] is important here. They showed that general agreement with experimental branching ratios can be obtained for the heavy (but not light) rare earths if the *4f* orbital moment is switched off. This indicates that the 5*d* spin-orbit coupling leads to an intrinsic 5*d* orbital moment irrespective of the 4*f* orbital moment. This is a very useful observation. While it is not physical (obviously, it means the calculated total magnetic moments disagree strongly with experiment), it clearly indicates that the branching ratios are very sensitively dependent on the intrinsic 5*d* spin-orbit coupling. However, we calculate magnetic moments in good agreement with experiment by including the 4*f* orbital moment. In our previous work, we calculated both Hund's rules compliant

$(J = L + S)$ and non-Hund's rules compliant $(J = L - S)$ $5d$ orbital moments. The results clearly indicated that the $5d$ unoccupied orbital moment depends strongly on the $4f$ orbital moment. Our calculated occupied $5d$ moments scale linearly with the de-Gennes factor confirming that the $5d$ polarization is governed by $4f$-$5d$ exchange. However, the positive peaks at 0.6 eV in the unoccupied spin-polarized DOS for Gd to Tm do not scale with the de-Gennes factor but rather with the $4f$ spin moment (or number of unoccupied $4f$ electron levels), which gives further weight to our argument that these peaks arise from antiparallel $4f/5d$ spin hybridization. Although the low-energy $E1$ peaks in the orbital DOS for Gd to Tm vary monotonically with the $4f$ orbital polarization, the relationship is nonlinear. The orbital contribution to the XRMS line shape is thus partly due to an intrinsic d orbital moment but also partly due to one induced by d hybridization with the minority-spin $4f$ states, which shows a dependence on the specific orbital content of those f spin states. While in XMCD and XRIS experiments these hybridized features should integrate to zero, in XRMS experiments, both the hybridized peaks and their closure feature contribute to the spectra. In Er and Tm, these features become the dominant contribution to the spin and orbital unoccupied DOSs, and

this may be the reason why the calculations in Ref. 26 underestimate the experimental branching ratios for these two elements.

We conclude that the low-energy $E1$ features in XRIS and XRMS spectra are associated with both spin and orbital moments generally. Although it is clear that the total $5d$ occupied moments are governed by the $4f$-$5d$ exchange, the specific line shape of the unoccupied moments contains additional contributions from f-d hybridization that are not indicative of the occupied $5d$ polarization. The f-d hybridization must also play a part in determining the indirect exchange interaction that is responsible for the cooperative magnetism in these elements. Clearly, there is further work to be done before a full understanding of magnetism in these elements is fully and quantitatively understood.

[1] M. Blume, J. Appl. Phys. **57**, 3615 (1985).

[2] D. Gibbs, D. R. Harshman, E. D. Isaacs, D. B. McWhan, D. Mills, and C. Vettier, Phys. Rev. Lett. **61**, 1241 (1988).

[3] D. Gibbs, G. Grübel, D. R. Harshman, E. D. Isaacs, D. B. McWhan, D. Mills, and C. Vettier, Phys. Rev. B **43**, 5663 (1991).

[4] J. P. Hannon, G. T. Trammell, M. Blume, and D. Gibbs, Phys. Rev. Lett. **61**, 1245 (1988).

[5] J. P. Hill and D. F. McMorrow, Acta Crystallogr. Sec. A **52**, 236 (1996).

[6] A. Mirone, L. Bouchenoire, and S. D. Brown, Acta Crystallogr. Sec. A **63**, 348 (2007).

[7] G. Schütz, W. Wagner, W. Wilhelm, P. Kienle, R. Zeller, R. Frahm, and G. Materlik, Phys. Rev. Lett. **58**, 737 (1987).

[8] P. Fischer, G. Schutz, S. Stahler, and G. Weisinger, J. Appl. Phys. **69**, 6144 (1991).

[9] F. Baudelet, C. Giorgetti, S. Pizzini, C. H. Brouder, E. Dartyge, A. Fontaine, J. P. Kappler, and G. Krill, J. Electron Spectrosc. Relat. Phenom. **62**, 153 (1993).

[10] M. H. Krisch, C. C. Kao, F. Sette, W. A. Caliebe, K. Hamalainen, and J. B. Hastings, Phys. Rev. Lett. **74**, 4931 (1995).

[11] F. Bartolome, J. M. Tonnerre, L. Seve, D. Raoux, J. Chaboy, L. M. Garcia, M. Krisch, and C. C. Kao, Phys. Rev. Lett. **79**, 3775 (1997).

[12] C. Detlefs, A. H. M. Z. Islam, A. I. Goldman, C. Stassis, P. C. Canfield, J. P. Hill, and D. Gibbs, Phys. Rev. B **55**, R680 (1997).

[13] S. D. Brown, P. Strange, L. Bouchenoire, B. Zarychta, P. B. J. Thompson, D. Mannix, S. J. Stockton, M. Horne, E. Arola, H. Ebert, Z. Szotek, W. M. Temmerman, and D. Fort, Phys. Rev. Lett. **99**, 247401 (2007).

[14] A. I. Goldman, B. N. Harmon, Y. B. Lee, and A. Kreyssig, Phys. Rev. Lett. **102**, 129701 (2009); S. D. Brown, P. Strange, L. Bouchenoire, B. Zarychta, P. B. J. Thompson, D. Mannix, S. J. Stockton,

M. Horne, E. Arola, H. Ebert, Z. Szotek, W. M. Temmerman, and D. Fort, *ibid.* **102**, 129702 (2009).

[15] J. Strempfer, D. Hupfeld, J. Voigt, G. Bihlmayer, A. I. Goldman, and Th. Bruckel, J. Phys.: Condens. Matter **20**, 445208 (2008).

[16] L. Bouchenoire, A. Mirone, S. D. Brown, P. Strange, T. Wood, P. Thompson, D. Fort, and J. Fernández-Rodríguez, New J. Phys. **11**, 123011 (2009).

[17] J. Bohr, D. Gibbs, and K. Huang, Phys. Rev. B **42**, 4322 (1990).

[18] M. K. Sanyal, D. Gibbs, J. Bohr, and M. Wulff, Phys. Rev. B **49**, 1079 (1994).

[19] D. B. McWhan, E. D. Isaacs, P. Carra, S. M. Shapiro, B. T. Thole, and S. Hoshino, Phys. Rev. B **47**, 8630 (1993).

[20] S. D. Brown, L. Bouchenoire, D. Bowyer, J. Kervin, D. Laundy, M. J. Longfield, D. Mannix, D. F. Paul, A. Stunault, P. Thompson, M. J. Cooper, C. A. Lucas, and W. G. Stirling, J. Synchrotron Radiat. **8**, 1172 (2001).

[21] H. L. Skriver, in *The LMTO Method*, Springer Series in Solid State Science, Vol. 41, edited by M. Cardona, P. Fulde, and H.-J. Queisser (Springer-Verlag, Berlin, 1984), p. 65.

[22] W. M. Temmerman, A. Svane, Z. Szotek, and H. Winter, in *Electronic Density Functional Theory: Recent Progress and New Directions*, edited by J. F. Dobson, G. Vignale, and M. P. Das (Plenum, New York, 1997), p. 327.

[23] P. Strange, A. Svane, W. M. Temmerman, Z. Szotek, and H. Winter, Nature (London) **399**, 756 (1999).

[24] E. Arola, P. Strange, and B. L. Gyorffy, Phys. Rev. B **55**, 472 (1997).

[25] E. Arola, M. Horne, P. Strange, H. Winter, Z. Szotek, and W. M. Temmerman, Phys. Rev. B **70**, 235127 (2004).

[26] Y. Lee, J. W. Kim, A. I. Goldman, and B. N. Harmon, J. Appl. Phys. **97**, 10A311 (2005).